# Ageing impairs the regenerative capacity of regulatory T cells in central nervous system remyelination

Alerie Guzman de la Fuente[1,2,3*], Marie Dittmer[1], Elise Heesbeen[1,4], Nira de la Vega Gallardo[1], Jessica White[3], Andrew Young[1,5], Katie Mayne[1,6], John Falconer[1,7], Christopher E. McMurran[8,9], Mohammed Innayatullah[1], Rebecca Ingram[1], Vijay Tiwari[1], Rosana Penalva[1], Yvonne Dombrowski[1] and Denise C. Fitzgerald[1*]

[1]Wellcome-Wolfson Institute for Experimental Medicine, Queen's University Belfast, Belfast, BT9 7BL, Northern Ireland, UK.

[2]Institute for Health and Biomedical Sciences of Alicante (ISABIAL), Alicante, 03010, Spain.

[3] Institute of Neuroscience of Alicante CSIC-UMH, San Juan de Alicante, 03550, Spain.

[4]Current address: Division of Pharmacology, Institute for Pharmaceutical Sciences, Utrecht University, Utrecht, The Netherlands.

[5] Current address Patrick G Johnston Centre for Cancer Research, Queen's University Belfast, Belfast, BT9 7BL, Northern Ireland, UK

[6]Current address: Department of Pathology and Laboratory Medicine, University of British Columbia, G227-2211 Wesbrook Mall, Vancouver, BC, V6T 2B5, Canada.

[7] Current address: CRUK Beatson Institute, G61 1BD, Glasgow, UK

[8] Department of Clinical Neurosciences, University of Cambridge, Cambridge, UK

[9] Department of Medical Epidemiology and Biostatistics, Karolinska Institute, Stockholm, Sweden

*Corresponding authors:

Denise C. Fitzgerald, d.fitzgerald@qub.ac.uk

Alerie G. de la Fuente, guzman_ale@isabial.es

**Abstract**

Myelin regeneration (remyelination) is essential to prevent neurodegeneration in demyelinating diseases such as Multiple Sclerosis but its efficiency declines with age. Regulatory T cells (Treg) recently emerged as critical players in tissue regeneration, including remyelination. However, the effect of ageing on Treg-mediated regenerative processes is poorly understood. Here, we show that expansion of aged Treg does not rescue age-associated remyelination impairment due to an intrinsically diminished capacity of aged Treg to promote oligodendrocyte differentiation and myelination. This decline in regenerative Treg functions can be rescued by a young environment. We identified Melanoma Cell Adhesion Molecule 1 (MCAM1) and Integrin alpha 2 (ITGA2) as novel candidates of Treg-mediated oligodendrocyte differentiation that decrease with age. Our findings demonstrate that ageing limits the neuroregenerative capacity of Treg, likely limiting their remyelinating therapeutic potential in aged patients and describe two novel mechanisms implicated in Treg-driven remyelination that may be targetable to overcome this limitation.

## Introduction

Myelin is critical to the metabolic support and function of axons in the central nervous system (CNS)[1]. CNS myelin is produced by oligodendrocytes and damage to oligodendrocytes or myelin causes neurological impairment[2–4]. Myelin regeneration (remyelination) is highly neuroprotective and holds potential to restore lost function for patients with demyelinating diseases such as Multiple Sclerosis (MS)[5–7]. Like most regenerative processes, remyelination efficiency declines with age[8,9], contributing to age-associated disease progression and the accumulation of irreversible disability[10]. Despite the critical neuroprotective role of remyelination, there are currently no approved remyelination-enhancing therapies, a key unmet medical need. Thus, understanding how ageing alters the different cellular mechanisms governing myelin regeneration is key to overcoming age-associated

remyelination failure. This holds potential to prevent neuronal loss and the accumulation of irreversible cognitive, sensory and motor disabilities.

Regulatory T cells (Treg) have recently emerged as key cellular players in tissue regeneration due to both anti-inflammatory functions and capacity to modulate tissue-resident stem cell differentiation[11,12]. Similar crosstalk has also been described in the CNS, where we and others showed that Treg promote oligodendrocyte progenitor cell (OPC) differentiation and CNS remyelination[13–15]. The discovery of pro-remyelinating functions of Treg opened a new therapeutic avenue to prevent remyelination decline and associated neurodegeneration. However, whether this important neuroregenerative function of Treg is impaired with age remains unknown. Understanding how ageing affects myelin-regenerative functions of Treg is essential to determine the relevance and suitability of potential Treg-based pro-remyelination therapies in patients of advanced age in MS and other demyelinating diseases.

Here, we show that ageing impairs the capacity of natural Treg to drive OPC differentiation *in vitro* and myelination *ex vivo*. Surprisingly, this defect was reversible in a young remyelinating environment *in vivo*. Transcriptomic comparison of young and aged Treg identified Melanoma Cell Adhesion Molecule 1 (MCAM1) and Integrin alpha 2 (ITGA2) as novel candidates of Treg-mediated OPC differentiation that decrease with age. This study identifies Treg-driven OPC differentiation as a novel remyelination mechanism that is impaired by ageing and identifies potential therapeutic targets to promote CNS remyelination.

## Results

### Expansion of Treg does not rescue impaired OPC differentiation in aged mice

We first examined murine Treg frequency with age, and in agreement with previous studies[16,17], found increased numbers and proportions of Treg in aged mice compared to young mice (**Fig. 1 A-D, Sup. Fig. 1 A**). We next verified that OPC differentiation into $CC1^+$ oligodendrocytes is impaired with ageing *in vivo* as previously reported[9,18] (**Fig. 1 E**), despite the endogenous increase in

Treg proportions with age. The impairment in oligodendrocyte differentiation with age was not rescued by further expanding Treg numbers in aged mice *in vivo* using IL-2/anti-IL-2 administration (**Fig 1 F-I**). Hence, we hypothesised that the myelin-regenerative capacity of Treg may be intrinsically impaired in aged Treg, irrespective of Treg frequency.

**Aged Treg demonstrate an impaired intrinsic myelin-regenerative capacity**

To compare the capacity of young and aged Treg to support the process of myelin regeneration, we first investigated effects on oligodendrocyte development. To do this, we isolated natural Treg from the spleens and lymph nodes of young (3-4 months) and aged (14-18 months) mice (**Sup. Fig. 1 A,B**) and co-cultured these Treg with neonatal murine OPCs. While neither young nor aged Treg modified OPC proliferation *in vitro* (**Fig. 2 A, B**), young Treg significantly increased OPC differentiation into myelin basic protein- (MBP) expressing oligodendrocytes, in agreement with our previous findings of Treg secretome[13,19]. Aged Treg however, did not enhance OPC differentiation demonstrating an impairment in their capacity to support this vital step in the process of myelin regeneration (**Fig. 2 C-E**).

To determine if the inability of aged Treg to support OPC differentiation was functionally relevant to the process of myelin production, we compared the capacity of young and aged Treg to drive myelin ensheathment of axons *ex vivo.* To do this, we co-cultured murine organotypic brain slices with young or aged Treg for 7 days. Young Treg significantly enhanced axonal myelination compared to control slices as described before[13]. However, aged Treg failed to significantly increase myelination in brain slices compared to controls, demonstrating an impairment in the capacity of aged Treg to drive myelin production (**Fig. 2 F, G**).

**Myelin-regenerative capacity of aged Treg is restored in a young environment**

We previously reported that Treg depletion using diphtheria toxin (DT) in B6.129(Cg)-*Foxp3*$^{tm3(DTR/GFP)Ayr}$/J (FoxP3-DTR)[20] mice impaired OPC differentiation and remyelination, which was

rescued by the administration of wild type Treg[13]. Thus, we next compared the regenerative capacity of young and aged Treg in a model of lysolecithin-induced spinal cord myelin damage *in vivo.* Following endogenous GFP$^+$ Treg depletion (**Sup. Fig. 1 C, D**), we administered wild type (GFP$^-$) young or aged Treg intraperitoneally and confirmed comparable detection of adoptively transferred Treg in each group (**Sup. Fig. 1 E, F**). We next compared the neuroregenerative capacity of adoptively transferred young and aged wild type Treg to enhance OPC differentiation during remyelination (**Fig. 3 A**). We did not observe any differences in the burden of damage for each experimental group, indicated by the lesion area (**Sup. Fig. 1 H**). There was also no difference in the number of oligodendrocyte lineage cells, quantified by Olig2 immunostaining (**Fig. 3 B-D**), or proliferating OPCs (Olig2$^+$Ki67$^+$) at 14 days post-lesion (dpl) (**Sup. Fig. 1 G, I, J**). As before[13], Treg depletion impaired OPC differentiation into CC1$^+$ and ASPA$^+$ oligodendrocytes, which was rescued by adoptive transfer of wild type young Treg. Unexpectedly however, aged Treg injected into young Treg-depleted mice also rescued impaired OPC differentiation, comparable to young Treg, (**Fig. 3 B, C, E, F**). To determine if aged Treg not only rescued OPC differentiation but also restored remyelination, we examined axonal wrapping through the quantification of circular myelin basic protein (MBP$^+$) patterns around neurofilament-H$^+$ (NFH$^+$) axons as an early indication of axonal remyelination. Both, young and aged Treg administered to Treg-depleted mice, restored axonal wrapping to levels comparable to non-depleted controls (**Fig. 3 G-J**). These findings suggest that the age-induced defect of neuroregenerative Treg functions observed *in vitro/ex vivo* is reversible in a young systemic environment *in vivo*, and therefore, potentially therapeutically targetable.

**Ageing significantly alters Treg transcriptome**

We next sought to identify how ageing impairs the myelin regenerative functions of Treg by examining gene expression differences in natural Treg purified from young and aged female mice. RNA sequencing (RNAseq) analysis showed that young and aged Treg clustered separately (**Fig. 4 A, C**) as shown in the literature[21,22] and identified 1423 upregulated and 302 downregulated mRNA transcripts

in aged Treg compared to young Treg (**Fig. 4 B**). However, there was no difference in the expression of classic Treg markers such as *Foxp3*, *Cd4* or *Il2ra* (**Sup. Fig. 2 B**). Gene Ontology (GO) analysis identified that the differentially expressed genes were associated with pathways linked to the adaptive immune response, lymphocyte-mediated immunity, phagocytosis, cell-surface receptor signalling and membrane invagination (**Fig. 4 D)**. Genes that were upregulated with ageing were enriched for the following GO biological processes: extracellular matrix organisation, cell migration, synapse assembly, axonal guidance, cell adhesion and inflammatory and immune responses (**Fig. 4 E**). On the other hand, mRNA transcripts that were downregulated in aged Treg were associated with defence responses to virus, B cell proliferation and protein folding GO biological processes (**Fig. 4 E)** (GO cellular component, GO Molecular function and Kyoto Encyclopedia of Genes and Genome (KEGG) database pathways analysis is shown in **Sup. Fig. 2**). To identify potential mechanisms underlying how ageing may impair myelin regenerative functions of Treg, we examined expression of genes associated with the Treg tissue repair programme described recently for skin, colon, lung and adipose tisse[23]. Unexpectedly, most of the 31 Treg tissue repair programme hallmark/signature genes[23] were in fact upregulated with ageing, except for *Klrb1, Ccr5, Selplg, Bach2, Rad50, Tfrc, Cd84 and Cd164* (**Fig. 4 F, G**). No difference in expression was detected in these hallmark genes between male and female natural Treg, showing that gender does not alter the expression of genes associated with the tissue repair programme (**Sup. Fig. 2 C, D**). These data suggest that the mechanism(s) involved in Treg-driven myelin regeneration capacity that are lost with ageing, are likely different to mechanisms from the Treg tissue repair programme described by Delacher et al[23].

**Mcam and Itga2 are associated with Treg capacity to drive oligodendrocyte formation**

To narrow down age-induced changes in Treg that diminish their capacity to induce OPC differentiation, we first investigated whether the putative mechanisms are soluble or contact-mediated; the latter being suggested by the close physical association of Treg with OPCs observed in co-cultures (**Fig. 5A**). Young natural Treg were co-cultured either directly in contact with OPC, or in

the same well but separated using a transwell, which allowed for the exchange of secreted molecules but not direct OPC-Treg contact. While young Treg co-cultured directly with OPCs enhanced OPC differentiation into MBP$^+$ oligodendrocytes, this pro-differentiating effect was lost when Treg were physically separated from OPCs (**Fig. 5 B, C**). To identify potential cell-to-cell contact mechanisms responsible for Treg-driven OPC differentiation that may be lost with ageing, we combined our aged Treg RNA sequencing data with a publicly available RNAseq dataset that compares between OPCs, newly differentiated and differentiated oligodendrocytes[24]. We hypothesised that ligand-receptor interactions between Treg and plasma membrane receptors enriched in OPCs underlie the pro-differentiation effect of Treg on OPC. We prioritised ligand-receptor partnerships between Treg and OPCs that were impacted by ageing, to identify mechanisms that could explain the lost myelin regenerative capacity of aged Treg. We then performed a protein-protein interaction analysis using String[25] (**Fig. 5 D**) and prioritised plasma membrane proteins that had the highest decrease in expression for aged Treg and the highest number of potential binding partners amongst OPC-enriched receptors compared to oligodendrocytes (**Fig. 5 E**). We identified the following key candidates: *Ccr7, Itga2* (CD49b), *Klrb1c* (NK1.1), *Ly6c1, Mcam* (CD146) and *Sell* (CD62L) (**Fig. 5 D-F**). Next, we used a loss-of-function approach to investigate whether these candidates may confer the lost regenerative capacity of aged Treg, namely, CD62L, NK1.1, LY6C, MCAM (CD146) and ITGA2 (CD49b). Of these five targets, antibody-mediated blocking of MCAM (CD146) and ITGA2 (CD49b) on Treg prior to Treg-OPC co-culture inhibited the capacity of young Treg to drive OPC differentiation *in vitro* as indicated by the fold change in the percentage of MBP+ cells and the MBP+ area per well (**Fig. 5 G-I, Sup. Fig. 2 H, I**). This suggests that MCAM and ITGA2 are previously unidentified mediators of pro-remyelinating functions of Treg and are downregulated with age.

## Discussion

Ageing is one of the strongest risk factors associated with the transition between relapsing-remitting to secondary progressive MS[10], a phase that is characterised by the accumulation of neurodegeneration and irreversible disability. This is partly due to impaired remyelination with age[8,9]. Several factors have been linked to age-associated myelin regeneration failure, such as impaired myelin debris phagocytosis by microglia and macrophages[26–28] and reduced capacity of OPCs to differentiate into myelin-forming oligodendrocytes[18,29]. Therapies that enhance remyelination and prevent age-related neurological decline are an urgent unmet need. Beyond their classic immune-modulatory and anti-inflammatory role, Treg have recently emerged as key regulators of tissue homeostasis and regeneration in several tissues[27], including the CNS, where we have previously identified Treg as key promoters of remyelination[13]. However, how ageing affects the capacity of Treg to enhance myelin regeneration had not been addressed.

Peripheral Treg increase with age[16,21,30], a somewhat paradoxical finding given the tissue-regenerative functions of Treg and the impairment of tissue regeneration with age. Here, we further expanded the murine Treg population *in vivo* and showed that despite this increased cell number, aged-associated remyelination failure was not rescued. These data suggest that with ageing, Treg have an intrinsically impaired myelin regenerative capacity. Ageing is known to enhance Treg senescence, limit Treg proliferation[16,21] and there are conflicting reports on the effect of ageing on Treg immunosuppressive capacity[16,21]. Additionally, previous work on muscle regeneration showed that aged Treg have an impaired migratory capacity that hinders muscle regeneration[31]. In a model of influenza infection, aged Treg demonstrated an impaired capacity to support lung repair, which was associated with a cell autonomous impairment in their regenerative programme[22]. Here, we sought to determine whether aged Treg have an intrinsically impaired regenerative capacity to drive CNS myelin regeneration combining *in vitro, ex vivo* and *in vivo* approaches.

Purified aged Treg failed to significantly enhance OPC differentiation into MBP-expressing oligodendrocytes or the myelination of cerebellar slices, which is in striking contrast to young Treg, which robustly drove both biological processes. These data suggest that ageing is associated with a

cell-intrinsic impairment of the regenerative capacity of Treg in CNS myelin regeneration. Given that IL-2-mediated Treg expansion *in vivo* is in clinical trial for MS (clinical trial number NCT02424396), our findings are of translational importance as they suggest that Treg expansion as a potential pro-remyelination therapy may be limited in older populations.

We next investigated whether the regenerative capacity of aged Treg could be restored, and therefore therapeutically targetable. Surprisingly, aged Treg rescued OPC differentiation and myelin wrapping similarly to that of young Treg in an *in vivo* model of young spinal cord remyelination. In contrast to findings in the lung[22], the CNS remyelinating capacity of Treg can be partially restored by a young environment. Previous studies identified a tissue repair transcriptomic signature in the skin, adipose tissue, and the lung[23]. Unexpectedly, very few of these hallmark Treg tissue repair genes were downregulated in aged Treg in our transcriptomic profiling studies. These data indicate that although some Treg regenerative mechanisms may be common across tissues, other mechanisms may be tissue-specific or process- specific[32].

We recognised that the impairment of myelin regenerative Treg functions with age presented a new avenue to discover novel mechanisms of how Tregs support CNS remyelination and the potential to identify new therapeutic targets to boost remyelination. Indeed, using a combined approach of Treg/OPC transcriptomic dataset cross-refencing with *in vitro* antibody blocking assays, we identified MCAM and ITGA2 as novel candidate mediators of Treg-driven OPC differentiation. These two candidates are downregulated in aged compared to young Treg, likely interact directly with OPCs and inhibit young Treg-driven OPC differentiation when blocked *in vitro*.

MCAM has previously been described as a cell-adhesion molecule contributing to brain inflammation by facilitating pathogenic T-cell extravasation into the CNS[33–35]. However, our study is, to our knowledge, the first report showing that MCAM signalling can promote OPC differentiation. Together with a recently published abstract examining Treg in MS patients (Poster 4[36]) these data also represent the first evidence that Treg express MCAM. We have also identified ITGA2 as a novel mediator of Treg-driven OPC differentiation that is decreased with age. This aligns with previous

reports showing that other integrins are involved in oligodendrocyte development[37] and shows that Treg are additional cellular contributors to integrin-mediated OPC differentiation.

Collectively, these studies have identified that ageing is associated with a cell-intrinsic impairment of the myelin-regenerative functions of Treg. This discovery increases the range of remyelination-associated mechanisms that are impaired with age[8,9,18,26–29,38]. Encouragingly, we have shown that this impairment can be rescued in a young environment *in vivo*. We have also identified two novel mediators of Treg-driven OPC differentiation, MCAM and ITGA2. The findings from this study identify novel mechanisms involved in CNS regeneration which may hold therapeutic potential for patients with demyelinating diseases.

## Methods

### Animals

All mice were on a C57BL/6J background and were either bred in-house or purchased from Charles River Laboratories, UK. Foxp3-DTR mice were a kindly provided by Prof. Alexander Rudensky (Memorial Sloan Kettering Institute, New York). Neonatal C57BL6/J P3-P7 pups were used for OPC and brain slice preparations, which were combined with natural Treg were isolated exclusively from young (3-4m) and aged (15-18m) C57BL6/J male mice for use with neonatal mixed sex pups. For *in vivo* Treg adoptive transfer studies, natural Treg were isolated from young (3-4m) and aged (15m) C57BL6/J female mice, and were injected into both, female and male recipient Foxp3-DTR mice (2-4m). To deplete Foxp3$^+$ cells in Foxp3-DTR mice, diphtheria toxin was administered as described below. All animal maintenance and experiments were done in accordance with the UK Home Office regulation (Project Licences 2789 and 2894) and were approved by the Queen's University Belfast's Animal Welfare and Ethical Review Committee.

### Lysolecithin-induced spinal cord demyelination *in vivo*

Spinal cord demyelination was induced as described previously[13]. In brief, demyelination was induced in the ventral white matter funiculus of the thoracic spinal cord (between vertebrae T11-12 or T12-13) by the injection of 1.2 µL of 1% (w/v) L-α-Lysophosphatidylcholine (Lysolecithin; Sigma-Aldrich) under general anaesthesia. At 10- or 14-days post lesion (dpl), mice were terminally anaesthetised with intraperitoneal (i.p.) pentobarbital injections and transcardially perfused with ice-cold phosphate buffered saline (PBS) followed by 4% paraformaldehyde (PFA) (Sigma-Aldrich). Spinal cords were dissected and immersed overnight in 4% PFA at 4 °C. Next, spinal cords were cryoprotected with 30% sucrose (Sigma-Aldrich) in PBS for 72h and snap-frozen in OCT (Tissue-Tek). Frozen spinal cords were cryosectioned at 12 µm thickness and immunostained as described below.

**_In vivo_ Treg expansion**

Aged mice (15m) were intraperitoneally injected with IL-2/anti-IL-2 antibody complexes to expand endogenous Treg[39]. In brief, murine IL-2 (1 µg; Peprotech) was mixed with anti-mouse IL-2 (5 µg; Bioxcell, Clone JES6-1A12) in PBS at 37 °C for 30 min. Each mouse was injected daily for 3 consecutive days with IL-2 (1 µg) and anti-IL-2 (5 µg) in 200µl of PBS. Adequate Treg expansion was assessed by flow cytometry as described below. Spinal cord demyelination was induced on the day after the third injection of IL-2/anti-IL-2, by injecting lysolecithin into the ventrolateral white matter as described above. Treg expansion was examined by flow cytometry as described below on day 10dpl, while OPC differentiation was examined at 10 dpl.

**_In vivo_ Treg depletion and adoptive transfer of wild type natural Treg**

Young (2-4m) male and female Foxp3-DTR mice were injected daily i.p. with diphtheria toxin (DT; 0.04 µg/g of body weight; Sigma, Cat. No. D0564) for 3 days prior to demyelination. To maintain endogenous Treg depletion during remyelination, DT (0.04 µg/g of body weight) was injected i.p. every fourth day. Control animals received 200 µl of saline i.p. Depletion was confirmed at the endpoint by flow cytometric analysis of endogenous $GFP^+$ natural Treg in blood, spleen, and lymph nodes (see

below). To adoptively transfer young (2-4m) and aged (15m) natural Treg to Treg-depleted mice, we immunomagnetically isolated natural Treg from wild type female mice using a $CD4^+$ and $CD25^+$ Treg isolation kit (STEMCELL Technologies) as described below. In the 24h prior to lysolecithin-induced demyelination, mice were injected i.p. with $10^6$ wild type natural Treg which are resistant to DT. Adequate reconstitution was evaluated by flow cytometry for Treg in lymph nodes at the endpoint (see below).

**OPC isolation and culture**

OPCs were isolated from P3-P7 mice based on A2B5 expression. Briefly, pups were culled by an overdose of pentobarbital (200 mg/mL, 20µl per mouse) and whole brain was dissected and placed in ice-cold Hibernate-A (ThermoFisher Scientific). Dissected brain was minced using scalpels, transferred to a 15mL tube, and centrifuged for 1 min at 100 g and 4 °C. Hibernate-A medium was aspirated, and the pellet was resuspended in 5 mL dissociation media containing 165U of Papain (Worthington) and DNAse type I (40 µg/mL; Worthington) in hibernate A for 30 min at 37 °C. Upon digestion papain was washed off with Hanks Buffered Salt Solution (HBSS) (ThermoFisher Scientific) and cells were centrifuged for 5 min at 300 g and 4 °C. The pellet was resuspended in 4 mL trituration buffer (Hibernate-A with 2% B27; ThermoFisher Scientific) and 2 mM sodium pyruvate (ThermoFisher Scientific) and gently triturated ten times using a 5 mL pipette. Tissue was left to settle for 2 min at room temperature (RT), and supernatant was transferred to a clean 50 mL tube through a 70 µm strainer (Corning). Remaining tissue was exposed to another 2 mL of trituration buffer and gently triturated using a glass polished pipette. After trituration, tissue was left to settle for 2 min at RT and supernatant was transferred to the tube through the 70 µm strainer. This step was repeated another time with a glass fire-polished pipette of decreased diameter and then with a 1 mL pipette. To further remove debris from the cell suspension, 11.5 mL of 90% Percoll (GE Healthcare) diluted in 10X PBS (ThermoFisher Scientific) was added and topped up to a final volume of 45 mL with Dulbecco's Modified Eagle's medium (DMEM) (ThermoFisher Scientific). The cell suspension was then centrifuged

312 at 800 g for 20 min at 4 °C. Upon centrifugation, the pellet was washed with HBSS and then
313 resuspended in 10 mL magnetic-activated cell sorting (MACS) buffer (Hibernate-A with 2 mM sodium
314 pyruvate, 2% B27, 0.5% BSA; ThermoFisher Scientific), 2 mM EDTA (Sigma-Aldrich) and 10 µg/mL
315 insulin (Sigma-Aldrich), and incubated for 30 min at 37 °C in a 10 cm petri dish coated with BSC1
316 Griffonia Simplicifolia Lectin (BSL1, 5 µg/mL)(Vektor Labs) to remove microglia. Then, the supernatant
317 was collected, and cells were counted and centrifuged at 300 g for 5 min at 4 °C. The pellet was
318 resuspended and incubated with 2 µg of A2B5 antibody (Millipore, Clone A2B5-105) in 500 µL of MACS
319 buffer per 10 million cells for 25 min on ice, with gentle resuspensions every 10 min. Cells were washed
320 with HBSS and spun at 300 g for 5min at 4 °C (Miltenyi Biotec). The pellet was resuspended and
321 incubated with 80 µL of MACS buffer and 20 µL of anti-IgM microbeads (Miltenyi Biotec) for 15 min.
322 Then, cell suspensions were centrifuged at 300 g for 5 min at 4 °C, resuspended in 0.5 ml MACS buffer
323 and placed in a MACS mini column (Miltenyi Biotec) on a MiniMACS Separator (Miltenyi Biotec) and
324 washed with 1.5mL MACS buffer. Once the liquid passed completely through the column, the column
325 was removed from the stand and placed in a new 15 mL tube, where 1 mL of OPC media was added
326 to the column and plunged through to elute the OPCs. OPC media contained DMEM, 2% B27, sodium
327 pyruvate (2 mM), insulin (5 µg/mL), Trace Elements B (0.01%; Corning), Forskolin (5 µM; Sigma-
328 Aldrich), Biotin (10 ng/mL; Sigma-Aldrich), Penicillin-streptomycin-glutamine (1%; ThermoFisher
329 Scientific), N-acetyl cysteine (60 µg/mL; Sigma-Aldrich) and 1% SATO stock solution. SATO stock
330 solution contained bovine serum albumin (BSA) fraction V (0.1 mg/mL; ThermoFisher Scientific),
331 sodium selenite (4 µg/mL; Sigma-Aldrich), putrescine (1.61 mg/mL; Sigma-Aldrich), apo-transferrin
332 (0.1 mg/mL; Sigma-Aldrich) and progesterone (4 µg/mL; Sigma-Aldrich). The purified population was
333 counted and diluted in OPC media for plating. OPCs were plated at a density of 3,000 cells per well in
334 96-well plates (Falcon) previously coated with poly-L-lysine (10 µg/mL; Sigma-Aldrich) and laminin (10
335 µg/mL; Sigma-Aldrich) diluted in DMEM. OPCs were plated with PDGFaa (20 ng/mL; Peprotech) and
336 NT-3 (10 ng/mL; Peprotech). The following day two thirds of the media was removed (100 µl) and 100
337 µl of fresh OPC media with PDGFaa (20 ng/mL) and NT3 (10 ng/mL) were added per well. Cells were

incubated at 37°C and 5% $CO_2$ for two days. On the third day, media was completely removed and 20,000 Treg in fresh media were added as indicated below.

For transwell assays, OPCs were selected with anti-PDGFRα panning. After microglia depletion in BSL1-coated petri dishes, the supernatant was transferred to PDGFRα panning plates and incubated at RT for 1 h. PDGFRα panning plates were coated with goat-anti-rat IgG (H+L) (7.5 µg/mL; ThermoFisher Scientific) in PBS with 0.2% BSA and rat anti-PDGFRα (1.5 µg/mL in PBS; BD Biosciences) with 0.2% BSA for 3 h. Supernatants were removed, cells were washed 5-8 times with PBS and the attached OPCs were scraped, counted, and replated in 24-well plates (Sarstedt) at 10,000 cells per well. On the third day *in vitro* 50,000 Treg were added either directly into the well with OPCs or in a transwell (Millipore) above the OPCs.

After 6 days of OPC-Treg co-culture cells were fixed for 15 min with 4% PFA and washed twice with PBS prior to immunostaining. Cells were blocked with 5% donkey serum (Sigma-Aldrich) with 0.1% Triton-X-100 (Sigma-Aldrich) in PBS for 1h at RT. OPCs were then stained overnight at 4 °C with primary antibodies diluted in blocking solution against Olig2 (1:500, Bio-techne), CNPase (1:500, Sigma-Aldrich, clone 11-5B), MBP (1:500, Millipore, clone 12), Ki67 (1:300, Abcam, clone SP6), NG2 (1:200, Millipore), and CD3 (1:500, eBioscience). Cells were then washed three times with PBS and incubated for 1 h at room temperature with secondary antibodies diluted in blocking buffer (Alexa fluor (AF) 488 donkey anti- rabbit (1:500; ThermoFisher Scientific), AF568 donkey-anti- rat (1:500; Abcam), AF647 donkey anti-mouse (1:500; Abcam), AF647 donkey anti-rabbit (1:500; ThermoFisher Scientific) and AF755 donkey anti-goat (1:500; ThermoFisher Scientific) and Höechst (1:10,000; Sigma-Aldrich). Cells were then washed with PBS three times and stored in 150 µL PBS/well for cell imaging.

Cell imaging was performed using the CellInsight CX5 high content imaging system (ThermoFisher Scientific) for 96-plates and EVOS for 24-well plates. Twenty-five separate fields of view of each well in 96-well plates and the cell populations of interest were quantified using CellInsight CX5 analysis software and the SpotCounts programme. For 24-well plates we imaged randomly 5 fields of view per well at 20X magnification and images were analysed manually with Fiji.

364

365 **Natural Treg isolation**

366 Young (2-4 m) and aged (15-18 m) male mice were culled by $CO_2$ overdose. Spleens and lymph nodes
367 were removed and mashed through a 70 µm strainer with a 2 ml syringe plunger. $CD4^+$ T cells were
368 immunomagnetically purified by negative selection according to manufacturer's instructions
369 (STEMCELL Technologies). Isolated $CD4^+$ T cells were then subjected to a $CD25^+$ cell isolation (STEMCELl
370 Technologies) using releasable magnetic spheres (STEMCELL Technologies) according to the
371 manufacturer's protocol. Purity was confirmed by flow cytometry for CD4, CD25 and Foxp3 (**Sup. Fig.**
372 **2A**). For i.p. injections in adoptive transfer experiments, cells were resuspended at $10^6$ cells per 200
373 µL in saline. For OPC-natural Treg co-cultures 20,000 natural Treg were resuspended in 150 µl of OPC
374 Brainphys-based media and added to OPCs in 96-well plates. For 24-well transwell plate experiments
375 50,000 natural Treg were resuspended in 250 µl OPC-BrainPhys media and added to transwells above
376 cultured OPCs. OPC BrainPhys-based media contains BrainPhys (STEMCELL Technologies), B27 (2%;
377 ThermoFisher Scientific), Glutamax (0.5 mM; ThermoFisher Scientific), N-acetyl-cysteine (60 µg/mL),
378 SATO (1:100, as described above) and insulin (5 µg/mL). In the case of brain slices, 50,000 Treg were
379 diluted in 5 µL of brain slice media and dropped directly onto brain slices.
380 For natural Treg mechanistic studies, OPCs and Treg were isolated as described above. Prior to OPC-
381 natural Treg co-culture, 120,000 Treg were transferred to a 1.5 mL microcentrifuge tube and
382 centrifuged at 400 g for 5 min at 4 °C. Treg were resuspended in 100 µL of PBS with 2% FCS and a
383 blocking antibody (20 µg/mL) or corresponding isotype were added per tube. Natural Treg were
384 incubated with the blocking antibody for 45 min on ice and then cells were washed with PBS and
385 centrifuged for 10 min at 400 g and 4 °C. Cells were resuspended in 900 µl of OPC BrainPhys-based
386 media (see above) and 20,000 Treg in 150 µL of media were added per well in 96-well plates. As
387 previously, Treg were co-cultured with OPCs for 7 days *in* vitro (DIV) and then fixed and stained as
388 described above. Blocking antibodies used were anti-NK1.1 PE (eBioscience, clone PK136), anti-CD62L-
389 APC (eBioscience, clone Mel14), anti-Ly6c1-APC (eBioscience, clone RB6-BC5), rat-isotype-APC

(eBioscience), anti-Itga2 (Abcam, clone EPR5788), anti-MCAM (Abcam, clone EPR3208) and rabbit-isotype (Vektor labs).

**Organotypic brain slice cultures**

Brainstem slices from male and female P3 C57BL/6J mice were prepared at 300 µm thickness using a McIlwain Tissue Chopper as described previously[13]. Slices were separated and placed on Millicell inserts in individual wells of a 24-well plate (Millipore) with 250 µl brain slice medium containing 46.6% minimum essential medium (ThermoFisher Scientific), 25% Earls balanced salt solution (Sigma-Aldrich), 25% heat-inactivated horse serum (Thermofisher Scientific), 1% penicillin-streptomycin (Thermofisher Scientific), 1% glutamax (Thermofisher Scientific) and 1.4% D-glucose (Sigma). Brain slices were incubated at 37 °C and 5% $CO_2$ overnight and then media was fully replaced. On day 3, media was changed again and 50000 young or aged Treg were added directly on top of each slice in a 5 µl droplet. Brain slices were cultured for a further 7 DIV, with media changes every other day. On day 10 (7 days post-treatment), brain slices were fixed with 4% PFA for 45 min and immunostained. In brief, brain slices were blocked for 2 h in 10% normal donkey serum (Sigma-Aldrich), 1 mM Hepes (Thermofisher Scientific), 1% BSA (ThermoFisher Scientific) and 0.5% Triton X-100 (Sigma-Aldrich) in PBS. Slices were incubated with primary antibodies for rat anti-MBP (1:500; Millipore, clone 12) and chicken anti-NFH (1:500; EncorBiotech, polyclonal) in blocking buffer at 4 °C for two overnights. Brain slices were then washed with PBS-0.01% triton three times for 30 min. Slices were incubated with secondary antibodies (AF488 donkey anti-chicken IgY (1:500; Abcam, polyclonal) and AF568 donkey anti-rat IgG (1:500; Abcam, polyclonal) in blocking buffer overnight at 4 °C. Brain slices were washed twice with PBS-0.01% triton and then incubated with Höechst stain (1:20000; Sigma-Aldrich) for 10 min. Slices were washed with PBS and mounted using fluoromount G (Thermofisher Scientific). Imaging was performed using a Leica SP8 confocal microscope, using a 63X oil objective and the Leica Navigator at 0.5 µm intervals over 10 µm. Four fields of view per brain slice were selected for imaging based on NFH and Höechst staining but blinded to MBP. To quantify myelination index, the area

stained by NFH, MBP and the colocalising area of $NFH^+MBP^+$ were measured per stack in Fiji[40] using a Fiji plug-in developed and kindly provided by the Williams laboratory at the University of Edinburgh[41]. Then, the ratio between total $NFH^+$ and $NFH^+MBP^+$ areas (myelination index) was calculated per z-stack and the average of the myelination index per slice was calculated.

**Flow cytometry**

Spleens and lymph nodes were mashed through a 70 µm strainer. For splenocytes, cells were exposed to red blood cell lysis buffer (STEMCELL Technologies) for 2 min at room temperature. Both, lymph nodes and splenocytes were then washed with PBS and centrifuged at 300 g for 5 min at 4°C. Cells were resuspended in 200 µL PBS and stained with a cell viability dye with eFluor 455-UV viability dye (1:2000; ThermoFisher Scientific) and cell surface stained with antibodies for CD4 (1:500; eBioscience, clone RM4.5) and CD25 (1:500; eBioscience, clone PC61.5) for 15 min at RT. Cells were washed with flow cytometry staining buffer (FCSB) (2% FCS in PBS) and centrifuged at 300 g for 5 min at 4 °C. Cells were then fixed with Fix & Perm A (ThermoFisher Scientific) for 10 min at RT. Fixative was washed off with FCSB and centrifuged at 300 g for 5 min at 4 °C. The pellet was resuspended in PBS and data were acquired on a FACSCanto II. In the natural Treg depletion experiment, presence of endogenous natural Treg was determined by the expression of GFP. To determine the purity of natural Treg isolations or the extent of natural Treg reconstitution by adoptive transfer, cells were washed and centrifuged for 5 min at 300 g and 4 °C. Cells were then resuspended in 100 µL Fix & Perm B (ThermoFisher Scientific) with an anti-Foxp3 antibody (1:100; eBioscience, clone FJK-16S) overnight at 4 °C. Cells were then washed with FCSB and centrifuged at 300 g and 4 °C for 5 min. Cells were then resuspended, data were acquired on a FACSCanto II and analysed using FlowJo software version 9.0 (BD). To calculate cell numbers, singlets were identified by FSC-H versus FSC-A and viable cells gated for CD3 and CD4, and subsequently CD25 and $Foxp3^+GFP^+$ and $Foxp3^+GFP^-$ cells. To evaluate young and aged Treg numbers in blood, 30 µL were incubated with 100 µL of the viability and cell surface antibody mix for 30 min at room temperature. Cells were then washed with FCSB and centrifuged at 300 g for 5 min at

4 °C. After resuspension, cells were fixed and lysed in 100 µL of OptiLyse B (Beckman Coulter) for 10 min at RT, washed with distilled water and then after 15 min, acquired on a FACSCanto II. After initial data acquisition, cells were centrifuged at 300 g for 5 min at 4 °C and incubated overnight with anti-Foxp3 antibody in Fix & Perm B, as described above. Cells were washed and data were acquired on a FACSCanto II.

**Immunofluorescence staining of CNS tissue**

Spinal cord sections were dried for 30 min at RT and washed for 10 min in PBS. For Olig2, Ki67, CC1 and ASPA staining, spinal cord sections underwent antigen retrieval at 85 °C for 10 min with 1X citrate buffer pH 6.0 (Sigma-Aldrich). Tissue sections were washed with PBS and permeabilised with 1% Triton-X-100 in PBS for 30 min at RT. Sections were washed with PBS and incubated with blocking solution (5% donkey serum; Sigma-Aldrich) diluted in TBS with 0.25% tween (Sigma-Aldrich) for 1h at RT. If spinal cord sections were incubated with a primary antibody raised in mouse (e.g. anti-CC1) sections underwent an additional 1 h blocking step at RT using Mouse on Mouse (M.O.M) blocking reagent (Vector labs) in 5% donkey serum. Then spinal cord sections were incubated with primary antibodies against Olig2 (1:500; Bio-Techne, polyclonal), anti-APC (1:400, Abcam, clone CC1), anti-ASPA (1:300, Millipore, polyclonal), anti-NFH (1:500; Abcam, polyclonal), anti-MBP (1:500; Millipore, clone 12) or anti-Ki67 (1:300; Abcam, clone SP6) overnight at 4 °C. Sections were washed with Tris-Buffered-Saline (TBS) (ThermoFischer Scientific) with 0.25% Tween (Sigma-Aldrich). Secondary antibodies including donkey anti-goat AF488, donkey anti-mouse AF568, donkey anti-rabbit AF647 (all 1:500; ThermoFisher Scientific), donkey anti-rat AF568 (1:500; Abcam), donkey anti-rabbit AF647 (1:500, Abcam) and Höechst (1:10000; Sigma-Aldrich) were added for 1 h at room temperature. Spinal cord sections were then washed with TBS-0.25% Tween twice and mounted with fluoromount G. Image acquisition was performed using the Leica TIRF and Leica DM5500 widefield fluorescent microscopes. Further image processing was performed in Fiji[40] software and analysis was undertaken

by blinded manual counting. For NFH and MBP wrapping analysis, images were quantified using Cell Profiler and Cell Profiler Analyst softwares[42,43].

**RNA sequencing and analysis**

Young (2-4m) and aged (16m-20m) natural Treg were isolated from spleen and lymph nodes by magnetic-activated cell sorting and purity was checked by flow cytometry as described above (**Sup. Fig. 3A**). Natural Treg were lysed in 0.5 mL of Trizol (Sigma-Aldrich) by vortexing and pipetting and frozen at -80 °C. RNA was extracted combining Trizol and Chloform isolations with RNAeasy micro kit columns (Qiagen). RNA concentration was determined using a Nanodrop, and RNA quality was assessed by Qubit measurement and in an RNA nanochip Bioanalyzer. Sequencing libraries were prepared using the Kapa Hyper Preparation kit with riboerase (Roche) following manufacturer's instructions. Sequencing was performed on the NovaSeq 6000 in a pair-end 75 base pair format and 80 million reads.

The raw sequencing data was checked for lower quality bases and adaptor sequences with FastQC and quality trimming was performed using CutAdapt[44]. The high-quality trimmed data were mapped on mm10 mouse reference genome using STAR aligner (v 2.7.0a)[45]. The quantification of each gene transcripts was performed with ensemble transcript annotation gtf file (GRCm38) using featureCounts tool (v 2.0.0)[46]. The resultant read counts matrix was analyse using DESeq2 (v1.38.1)[47] to identify differentially expressed genes between the young and aged natural Treg samples using Wald tests with the Bonferroni correction for multiple testing. The differentially expressed genes (DEG) with a multiple testing adjusted $p<0.05$ and fold change >2 were considered for further downstream analysis. These genes were subjected to gene ontology enrichment analysis using enrichGO function in clusterProfiler (v4.2) R package and DAVID (https://david.ncifcrf.gov). Over and underrepresented ontology terms were identified (p value <= 0.05 and Bonferroni correction p adjustment method). Next, enriched activated and suppressed functional pathways were identified using gseKEGG function in clusterProfiler with $p$ value$<0.05$.

493 Raw data files from RNAseq are available at the GEO database (accession number GSE218804).

494

495 **Bioinformatic analysis to identify putative Treg mechanisms**

496 To determine the molecular mechanisms associated with Treg-driven OPC differentiation that are
497 impaired with ageing, we combined our young and aged natural Treg RNA sequencing with data
498 obtained from Zhang *et al*. 2014 (GSE: 52564)[24]. We first extracted genes that were downregulated in
499 aged natural Treg and associated with the GO cellular component term "plasma membrane". We then
500 extracted the FPKM matrix and selected genes that were upregulated in OPC when compared with
501 newly myelinating oligodendrocytes and oligodendrocytes in the Zhang *et al*. database. We performed
502 GO cellular component analysis on those OPC-enriched genes and selected genes associated with the
503 GO term Apical Plasma Membrane. Then, both gene lists were subjected to a protein-protein
504 interaction analysis using the String open-source tool (www.string-db.org)[25]. Protein-protein
505 interactions within genes that were associated only with the natural Treg or only the OPC databases
506 were eliminated, and the remaining downregulated natural Treg membrane proteins were prioritised
507 considering their significance, fold change and the number of potential interactors enriched in OPCs.
508 Candidate genes were then selected based on their p-adjusted value, fold enrichment and the number
509 of interactions with OPC receptors.

510

511 **Statistical analysis**

512 All statistical analyses were performed in GraphPad Prism (GraphPad Software, Inc. version 9) or R.
513 First normality of datasets was assessed using Shapiro-Wilk and Kolmogorov-Smirnov tests. For
514 comparisons between 2 groups, such as young and aged Treg and OPC differentiation (Sup. Fig. 1),
515 unpaired two-tailed Student's t tests were used if data were normally distributed, and Mann-Whitney
516 U tests for non-parametric datasets. When more than two groups were analysed and datasets were
517 normally distributed, a one-way analysis of variance (ANOVA) was performed assuming equal
518 variances, followed by Sidak's multiple comparison test. When two factors were controlling the

519 outcome, such as replicates and treatments, 2-way ANOVA followed by Dunnet's comparison was
520 used. When datasets were was not normally distributed, a Kruskal-Wallis followed by Dunn's multiple
521 comparison test was used. For percentage data, arcsin conversion was performed to analyse the data
522 using parametric tests. For all statistical tests, differences were considered significant at $p<0.05$.
523
524 **Data and code availability**
525 Young and aged natural Treg RNA sequencing data will also be deposited at GEO (NCBI) with the
526 revised version.
527
528 **Figure legends**
529
530 **Figure 1: Expansion of Treg does not rescue impaired OPC differentiation in aged mice. A**) Flow
531 cytometric plot and **B**) quantification of natural Treg proportion, identified by CD4 and Foxp3
532 expression in young and aged mouse spleens (n=15-32, unpaired two-tailed Student's t test after
533 *arcsin* conversion). **C**) Flow cytometric plot and **D**) quantification showing the proportions of natural
534 Treg (endogenous GFP reporting Foxp3 expression in Foxp3-DTR mice) in aged blood compared to
535 young circulation (n=30-38 mice, unpaired two-tailed Student's t test after *arcsin* conversion). **E**) Bar
536 graph showing the density of $OLIG2^+CC1^+$ oligodendrocytes in young and aged lysolecithin-induced
537 demyelinating lesions at 14dpl (n=4 mice, unpaired Student's t test). **F**) Flow cytometric plot showing
538 CD25 and Foxp3 expression and the quantification of $CD25^+Foxp3^+$ natural Treg proportion in a $CD4^+$
539 T cell population from the spleen (**G**) and blood (**H**) of control aged mice and aged mice treated with
540 intraperitoneal injection of IL-2/anti-IL-2 complexes (n=3, unpaired two-tailed Student's t test after
541 *arcsin* conversion). **I**) Bar graph showing the quantification of $OLIG2^+CC1^+$ oligodendrocyte density at
542 10dpl in aged control and Treg-expanded mice (n=6-7, unpaired Student's t test).
543

**Figure 2: Aged natural Treg demonstrate impaired capacity to drive OPC differentiation and myelination *in vitro*.** Representative images of OPCs co-cultured with young and aged natural Treg and immunostained for OLIG2 (cyan) as a pan oligodendrocyte lineage marker, the proliferation marker Ki67 (magenta, **A**) and differentiation markers CNP (grey) and MBP (magenta) (**C**) (Scale bar = 100 µm). **B**) Quantification of OPC proliferation when co-cultured with young and aged natural Treg (n=6, 1-way ANOVA after *arcsin* conversion) **D**) Quantification of the proportion of OPCs reaching early stage-differentiation when exposed to young and aged natural Treg, as indicated by CNPase staining (n=9, 1-way ANOVA after *arcsin* conversion). **E**) Quantification of the proportion of OPCs expressing late-stage differentiation marker MBP in control and OPCs treated with young and aged natural Treg (n=9, 1-way ANOVA, Sidak's multiple comparisons test). **F**) Immunohistochemistry of control and young and aged Treg treated cerebellar slices (MBP, magenta and NFH, green, Scale bar = 100 µm). (**G**) Quantification of myelination index (ratio between MBP and NFH colocalization area and NFH area) in neonatal cerebellar slices (n=7, 1-way ANOVA after *arcsin* conversion, Sidak's multiple comparison tests).

**Figure 3: Myelin-regenerative capacity of aged Treg is restored in a young environment. A)** Diagram explaining the experimental design of *in vivo* Treg depletion, Treg adoptive transfer and spinal cord demyelination. Representative images of immunostaining identifying oligodendrocytes by the co-localisation of the pan-oligodendrocyte lineage marker OLIG2 (green) with CC1 (magenta, **B**) or ASPA (magenta, **C**) at 14 dpl (scale bar = 100 µm, demyelination area is highlighted by the white line). Bar graphs show the quantification of total number of oligodendrocyte lineage cells (**D**), as well as CC1-expressing (**E**) or ASPA-expressing (**F**) oligodendrocytes in the demyelinated lesions of PBS control mice, natural Treg-depleted mice and mice depleted of endogenous Treg that received young or aged natural Treg by adoptive transfer (n=7-9, 1-way ANOVA, Sidak's multiple comparisons test). **G**) Representative images of immunostaining for neurofilament-H (NFH, green) and MBP (magenta) to quantify myelin wrapping as an early marker of remyelination at 14 dpl (scale bar = 100 µm,

570 demyelination area is highlighted by the white line). Quantification shows the total number of axons
571 (**H**), the density of MBP wrapped axons (**I**) and the percentage of MBP-wrapped axons from the total
572 number of axons (**J**) (n=6-9, 1-way ANOVA, Sidak's multiple comparisons test).
573
574 **Figure 4: Ageing significantly alters natural Treg transcriptome. A**) Principal component analysis
575 demonstrating the clustering differences between young and aged natural Treg. **B**) Volcano plot
576 demonstrating 1456 genes upregulated and 302 genes downregulated genes in aged natural Treg
577 relative to young Treg. **C**) Heatmap demonstrating hierarchical clustering of the top 50 differentially
578 expressed genes between young and aged Treg. **D**) Graph showing the pathways enriched amongst
579 differentially expressed genes. **E**) Bar graph highlighting the GO biological processes associated with
580 genes that are upregulated or downregulated in aged Treg. **F**) Heatmap showing the normalised count
581 values for the Treg tissue repair programme identified by Delacher *et al*.[23] **G**) Graph showing the Treg
582 tissue repair programme signature genes score in aged and young natural Treg.
583
584 **Figure 5: *Mcam* and *Itga2* contribute to Treg-driven OPC differentiation and are downregulated in**
585 **aged Treg. A**) Representative images of immunostaining showing cell-to-cell contact between OPCs
586 and Treg in OPC-Treg co-cultures *in vitro*. OPCs are identified by the co-staining of OLIG2 (cyan) and
587 NG2 (grey), while Treg are identified by CD3 (red) (scale bar = 50 µm). **B**) Representative images of
588 immunostaining and **C**) quantification of MBP-expressing oligodendrocytes in control OPCs, OPCs
589 directly co-cultured with young Treg and OPCs cultured with young Treg in a transwell (n=6, 1-way
590 ANOVA after arcsin conversion, Sidak's multiple comparison's test). **D**) Diagram summarising
591 bioinformatic approaches to identify protein-protein interactions between OPCs and Treg. **E**) Graph
592 showing 21 protein candidates expressed in the Treg plasma membrane, that are downregulated in
593 aged Treg and have potential bindings partners enriched in OPCs vs oligodendrocytes. $Log_2$ Change, -
594 $Log_{10}$ (Padj) and the number of OPC binding partners are indicated (see legend). **F**) Bar graphs showing
595 RNAseq normalised count values for the top 6 candidates. **G**) Representative images of

596 immunostaining showing OPC differentiation in co-culture with young Treg in the presence or absence
597 of neutralising antibodies against candidate cell surface mediators (scale bar = 100µm). Bar graphs
598 showing the quantification of OPC differentiation measured by the fold change in percentage of $MBP^+$
599 cells (**H**) and $MBP^+$ area per well (**I**) (n=7, 2-way ANOVA, Dunnett's multiple comparison tests).
600
601 **Supplementary information**
602
603 **Supplementary Figure 1: Endogenous Treg depletion and reconstitution during lysolecithin- induced**
604 **demyelination *in vivo*. A**) Gating strategy followed to identify natural Treg. **B**) Bar graph showing
605 natural Treg isolation purity for *in vitro* experiments and *in vivo* adoptive transfer studies. Natural Treg
606 are identified by CD4 and CD25 expression (average 91% of the isolated cells for both young and aged
607 are $CD4^+CD25^+$) and by the expression of CD4 and Foxp3 (average 87% of the isolated cells are positive
608 for CD4 and Foxp3 in both young and aged mouse isolations) (n=14 independent isolations for
609 different adoptive transfer rounds, each pool comprises 2-8 different mice, Student's t test, after
610 *arcsin* conversion). **C**) Flow cytometric plot showing CD4 and GFP expression to identify endogenous
611 natural Treg in lymph nodes. **D**) Bar graph showing quantification for the proportion of endogenous
612 $GFP^+$ Treg within the $CD4^+$ T cell population in the lymph nodes of young Foxp3-DTR mice at 14dpl
613 (n=7-9, 1-way ANOVA, after *arcsin* conversion, Sidak's multiple comparisons test). **E**) Flow cytometric
614 plots showing CD25 and Foxp3 expression to detect Treg reconstitution in lymph nodes after adoptive
615 transfer. **F**) Bar graph quantification shows the proportion of $CD25^+Foxp3^+$ cells within the $CD4^+$ T cell
616 population present in the lymph nodes of young Foxp3-DTR mice at 14dpl (n=7-12, Kruskal Wallis and
617 Dunn's multiple comparisons test). **G**) Representative images of immunostaining showing proliferating
618 OPCs at 14 dpl (OLIG2 (green) and Ki67 (magenta)) (scale bar = 100 µm, demyelinated area is indicated
619 by the white line). Bar graph showing the areas of demyelination (**H**), the density of proliferating OPCs
620 in the lesion (**I**) and the proportion of oligodendrocyte lineage cells proliferating in response to
621 damage (**J**) (n=7-8 mice, 1 way ANOVA).

**Supplementary Figure 2: Downstream analysis of differentially expressed genes between young and aged natural Treg. A**) Bar graphs showing the purity of young and aged natural Treg subjected to RNA sequencing (on average 89% of $CD4^+$ cells were $Foxp3^+$, while 94% of $CD4^+$ cells were $CD25^+$) (n=4-6 mice, Mann-Whitney U test). **B**) Bar graph showing normalised counts of natural Treg marker transcripts *Foxp3*, *Cd4* and *IL2ra*. **C**) Heatmap and **D**) quantification of normalised count values of the Treg tissue repair programme in male and female Treg. Bar graphs showing the GO cellular component (**E**), molecular function (**F**) and KEGG pathways (**G**) enriched within the differentially expressed genes upregulated (magenta) and downregulated (purple) in aged Treg. Bar graphs showing the quantification of OPC differentiation in OPC and young Treg co-cultures in the presence or absence of neutralising antibodies against candidate cell surface mediators, measured by the fold change in the percentage of $MBP^+$ cells (**H**) and the fold change in $MBP^+$ area per well (**I**) (n=5-7, 2-way ANOVA, Dunnet's multiple comparisons test).

**Acknowledgements**

We acknowledge extensive technical support from Carmel McVicar, Maria P Athanasios and the staff of the animal facility. We thank A. Rudensky (Memorial Sloan Kettering Cancer Centre) for providing Foxp3-DTR mice. This work was supported by the Wellcome Trust (110138/Z/15/Z to DCF), Biotechnology and Biological Sciences Research Council (BB/J01026X/1 and BB/N003721/1, to DCF), ECTRIMS postdoctoral fellowship (to AGF), Wellcome ISSF fellowship (to AGF), Miguel Servet Fellowship from the Spanish Institute of Health Carlos III (CP21/00032 to AGF), The Leverhulme Trust (ECF-2014-390, to YD) and postgraduate studentship support from the Dept. for the Economy (Northern Ireland). We thank the laboratory of Anna Williams (University of Edinburgh) for the Fiji plug-in to analyse myelination index in brain slice cultures.

## Author contributions

Experiments were designed by A.G.F., D.C.F., Y.D. and V.T. Experiments were performed and/or analysed by A.G.F., M.D., E.H., N.V.G., J.W., A.Y., K.M., J.F., C.E.M., M.I., R.P., Y.D. and D.C.F. R.J.I. and C.E.M. provided advice on experimental design and interpretation. Manuscript was written by A.G.F. and D.C.F. with contributions from all authors. D.C.F and A.G.F. oversaw the study.

## References

1. Nave, K.-A. & Werner, H. B. Ensheathment and Myelination of Axons: Evolution of Glial Functions. *Annu Rev Neurosci* **44**, 1–23 (2021).

2. Griffiths, I. *et al.* Axonal swellings and degeneration in mice lacking the major proteolipid of myelin. *Science* **280**, 1610–1613 (1998).

3. Lappe-Siefke, C. *et al.* Disruption of Cnp1 uncouples oligodendroglial functions in axonal support and myelination. *Nat Genet* **33**, 366–374 (2003).

4. Love, S. Demyelinating diseases. *J Clin Pathol* **59**, 1151 (2006).

5. Bodini, B. *et al.* Dynamic Imaging of Individual Remyelination Profiles in Multiple Sclerosis. *Ann Neurol* **79**, 726–738 (2016).

6. Franklin, R. J. M. & ffrench-Constant, C. Regenerating CNS myelin — from mechanisms to experimental medicines. *Nat Rev Neurosci***18**, 753–769 (2017).

7. Lubetzki C. *et al*. Remyelination in multiple sclerosis: from basic science to clinical translation. *The Lancet Neurol* **19**, 678–688 (2020).

8. Shields, S., Gilson, J., Blakemore, W. & Franklin, R. Remyelination occurs as extensively but more slowly in old rats compared to young rats following fliotoxin-induced CNS demyelination. *Glia* **29**, 102 (2000).

9. Sim, F. J., Zhao, C., Penderis, J. & Franklin, R. J. M. The age-related decrease in CNS remyelination efficiency is attributable to an impairment of both oligodendrocyte progenitor recruitment and differentiation. *J Neurosci* **22**, 2451–2459 (2002).

10. Confavreux, C. & Vukusic, S. Age at disability milestones in multiple sclerosis. *Brain* **129**, 595–605 (2006).

11. Burzyn, D. *et al.* A special population of regulatory T cells potentiates muscle repair. *Cell* **155**, 1282–1295 (2013).

680 12. Ali, N. *et al.* Regulatory T Cells in Skin Facilitate Epithelial Stem Cell Differentiation. *Cell* **169**,
681 1119-1123.e11 (2017).

682 13. Dombrowski, Y. *et al.* Regulatory T cells promote myelin regeneration in the central nervous
683 system. *Nat Neurosci* **20**, 674–680 (2017).

684 14. McIntyre, L. L. *et al.* Regulatory T cells promote remyelination in the murine experimental
685 autoimmune encephalomyelitis model of multiple sclerosis following human neural stem cell
686 transplant. *Neurobiol Dis* **140**, 104868 (2020).

687 15. Shi, L. *et al.* Treg cell-derived osteopontin promotes microglia-mediated white matter repair
688 after ischemic stroke. *Immunity* **54**, 1527-1542.e8 (2021).

689 16. Garg, S. K. *et al.* Aging is associated with increased regulatory T-cell function. *Aging Cell* **13**, 441–
690 448 (2014).

691 17. Elyahu, Y. *et al.* Aging promotes reorganization of the CD4 T cell landscape toward extreme
692 regulatory and effector phenotypes. *Sci adv* **5**, eaaw8330 (2019).

693 18. Neumann, B. *et al.* Metformin Restores CNS Remyelination Capacity by Rejuvenating Aged Stem
694 Cells. *Cell Stem Cell* **25**, 473-485.e8 (2019).

695 19. Dittmer, M. *et al.* Characterization of a murine mixed neuron-glia model and cellular responses
696 to regulatory T cell-derived factors. *Mol brain* **11**, 25 (2018).

697 20. Kim, J. M., Rasmussen, J. P. & Rudensky, A. Y. Regulatory T cells prevent catastrophic
698 autoimmunity throughout the lifespan of mice. *Nat Immunol* **8**, 191–197 (2007).

699 21. Guo, Z. *et al.* DCAF1 regulates Treg senescence via the ROS axis during immunological ageing. *J*
700 *Clin Invest* **130**, 5893–5908 (2020).

701 22. Morales-Nebreda, L. *et al.* Aging imparts cell-autonomous dysfunction to regulatory T cells
702 during recovery from influenza pneumonia. *JCI Insight* **6**, e141690 (2021).

703 23. Delacher, M. *et al.* Single-cell chromatin accessibility landscape identifies tissue repair program in
704 human regulatory T cells. *Immunity* **54**, 702-720 (2021).

705 24. Zhang, Y. *et al.* An RNA-sequencing transcriptome and splicing database of glia, neurons, and
706 vascular cells of the cerebral cortex. *J Neurosci* **34**, 11929–11947 (2014).

707 25. Jensen, L. J. *et al.* STRING 8--a global view on proteins and their functional interactions in 630
708 organisms. *Nucleic Acids Research* **37**, D412-6 (2009).

709 26. Natrajan, M. S. *et al.* Retinoid X receptor activation reverses age-related deficiencies in myelin
710 debris phagocytosis and remyelination. *Brain* **138**, 3581–3597 (2015).

711 27. Linehan, E. *et al.* Aging impairs peritoneal but not bone marrow-derived macrophage
712 phagocytosis. *Aging cell* **13**, 699–708 (2014).

713 28. Cantuti-Castelvetri, L. *et al.* Defective cholesterol clearance limits remyelination in the aged
714 central nervous system. *Science* **359***, 684-688* (2018).

715 29. Segel, M. *et al.* Niche stiffness underlies the ageing of central nervous system progenitor cells.
716 *Nature* **350**, 1199–134 (2019).

717 30. Wang, W., Thomas, R., Oh, J. & Su, D. Accumulation of pTreg cells is detrimental in late-onset
718 (aged) mouse model of multiple sclerosis. *Aging Cell* **21**, e13630 (2022).

719 31. Kuswanto, W. *et al.* Poor Repair of Skeletal Muscle in Aging Mice Reflects a Defect in Local,
720 Interleukin-33-Dependent Accumulation of Regulatory T Cells. *Immunity* **44**, 355–367 (2016).

721 32. Muñoz-Rojas, A. R. & Mathis, D. Tissue regulatory T cells: regulatory chameleons. *Nat Rev*
722 *Immunol* **21**, 597-611 (2021).

723 33. Breuer, J. *et al.* Blockade of MCAM/CD146 impedes CNS infiltration of T cells over the choroid
724 plexus. *J Neuroinflamm* **15**, 236 (2018).

725 34. Zondler, L. *et al.* MCAM/CD146 Signaling via PLCγ1 Leads to Activation of β1-Integrins in Memory
726 T-Cells Resulting in Increased Brain Infiltration. *Front Immunol* **11**, 599936 (2020).

727 35. Larochelle, C. *et al.* Melanoma cell adhesion molecule–positive CD8 T lymphocytes mediate
728 central nervous system inflammation. *Ann Neurol.* **78**, 39–53 (2015).

729 36. ACTRIMS Forum 2020 - Poster Session 1. Poster 4. Zandee, S.E. *et al*. Can T Cell Migratory
730 Signature Predict MS Disease Progression? *Mult Scler J* **26**, 16–89 (2020).

731 37. Laursen, L. S., Chan, C. W. & ffrench-Constant, C. An Integrin-Contactin Complex Regulates CNS
732 Myelination by Differential Fyn Phosphorylation. *J Neurosci* **29**, 9174–9185 (2009).

733 38. Ruckh, J. M. *et al.* Rejuvenation of regeneration in the aging central nervous system. *Cell stem*
734 *cell* **10**, 96–103 (2012).

735 39. Webster, K. E. *et al.* In vivo expansion of T reg cells with IL-2–mAb complexes: induction of
736 resistance to EAE and long-term acceptance of islet allografts without immunosuppression. *J Exp*
737 *Medicine* **206**, 751–760 (2009).

738 40. Schindelin, J. *et al.* Fiji: an open-source platform for biological-image analysis. *Nat Methods* **9**,
739 676–682 (2012).

740 41. Zhang, H., Jarjour, A. A., Boyd, A. & Williams, A. Central nervous system remyelination in culture
741 — A tool for multiple sclerosis research. *Experimental Neurology* **230**, 138–148 (2011).

742 42. Stirling, D. R. *et al.* CellProfiler 4: improvements in speed, utility and usability. *Bmc Bioinformatics*
743 **22**, 433 (2021).

744 43. Dao, D. *et al.* CellProfiler Analyst: interactive data exploration, analysis and classification of large
745 biological image sets. *Bioinformatics* **32**, 3210–3212 (2016).

746 44. Martin, M. Cutadapt removes adapter sequences from high-throughput sequencing reads.
747 *Embnet J* **17**, 10–12 (2011).

748 45. Dobin, A. *et al.* STAR: ultrafast universal RNA-seq aligner. *Bioinformatics* **29**, 15–21 (2013).

749 46. Liao, Y., Smyth, G. K. & Shi, W. featureCounts: an efficient general purpose program for assigning
750 sequence reads to genomic features. *Bioinformatics* **30**, 923–930 (2013).

751 47. Love, M. I., Huber, W. & Anders, S. Moderated estimation of fold change and dispersion for RNA-
752 seq data with DESeq2. *Genome Biol* **15**, 550 (2014).

753

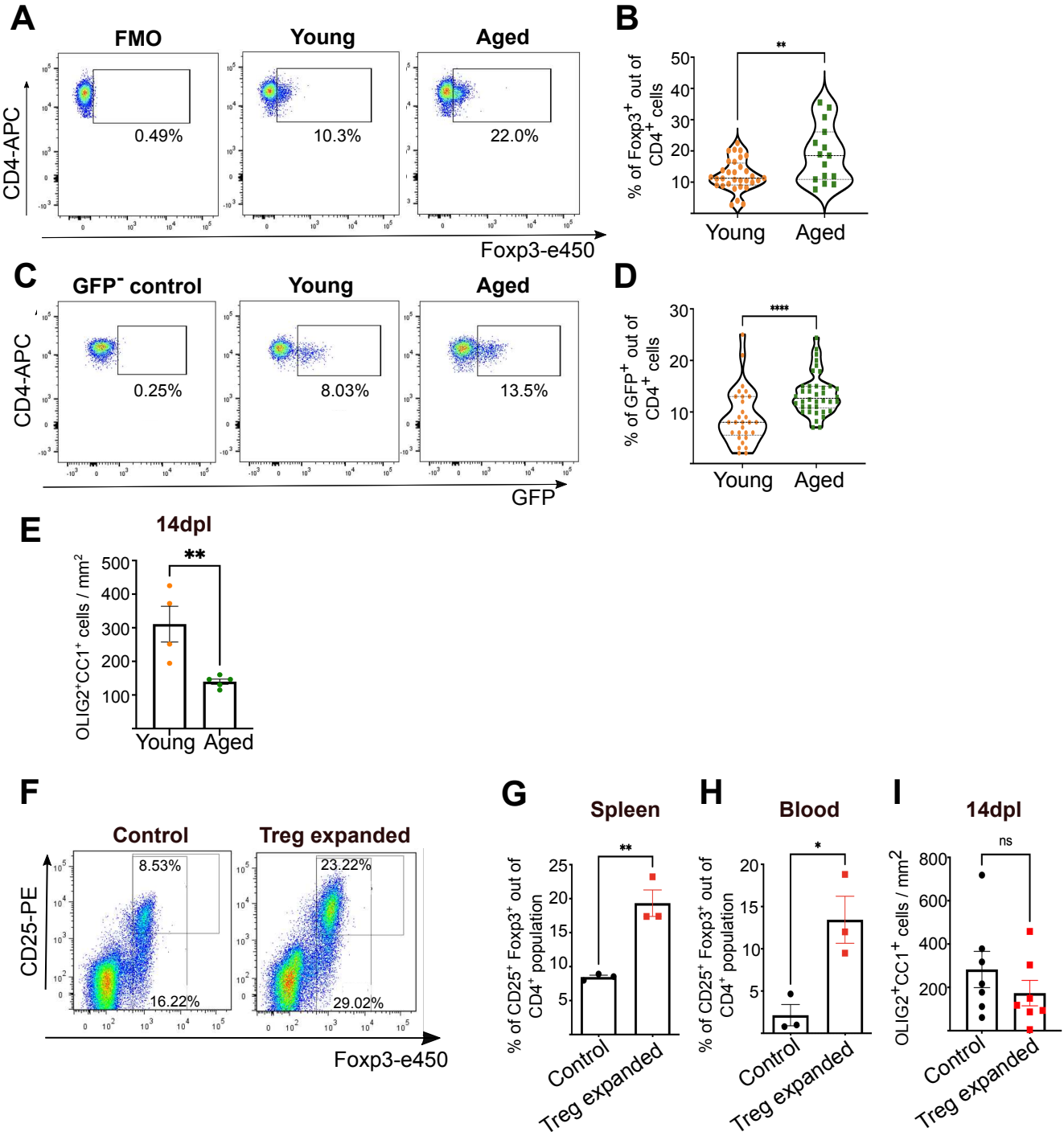


**Figure 1: Expansion of Treg does not rescue impaired OPC differentiation in aged mice.** **A**) Flow cytometric plot and **B**) quantification of natural Treg proportion, identified by CD4 and Foxp3 expression in young and aged mouse spleens (n=15-32, unpaired two-tailed Student's t test after *arcsin* conversion). **C**) Flow cytometric plot and **D**) quantification showing the proportions of natural Treg (endogenous GFP reporting Foxp3 expresion in Foxp3-DTR mice) in aged blood compared to young circulation (n=30-38, unpaired two-tailed Student's t test). **E**) Bar graph showing the density of OLIG2$^+$CC1$^+$ oligodendrocytes in young and aged lysolecithin-induced demyelinating lesions at 14dpl (n=4 mice, unpaired Student's t test). **F**) Flow cytometric plot showing CD25 and Foxp3 expression and the quantification of CD25$^+$Foxp3$^+$ natural Treg proportion in a CD4$^+$ T cell population from the spleen (**G**) and blood (**H**) of control aged mice and aged mice treated with intraperitoneal injection of IL-2/anti-IL-2 complexes (n=3, unpaired two-tailed Student's t test after arcsin c conversion). **I**) Bar graph showing the quantification of OLIG2$^+$CC1$^+$ oligodendrocyte density at 10dpl in aged control and Treg expanded mice (n=6-7, unpaired Student's t test).

**Fig. 1**

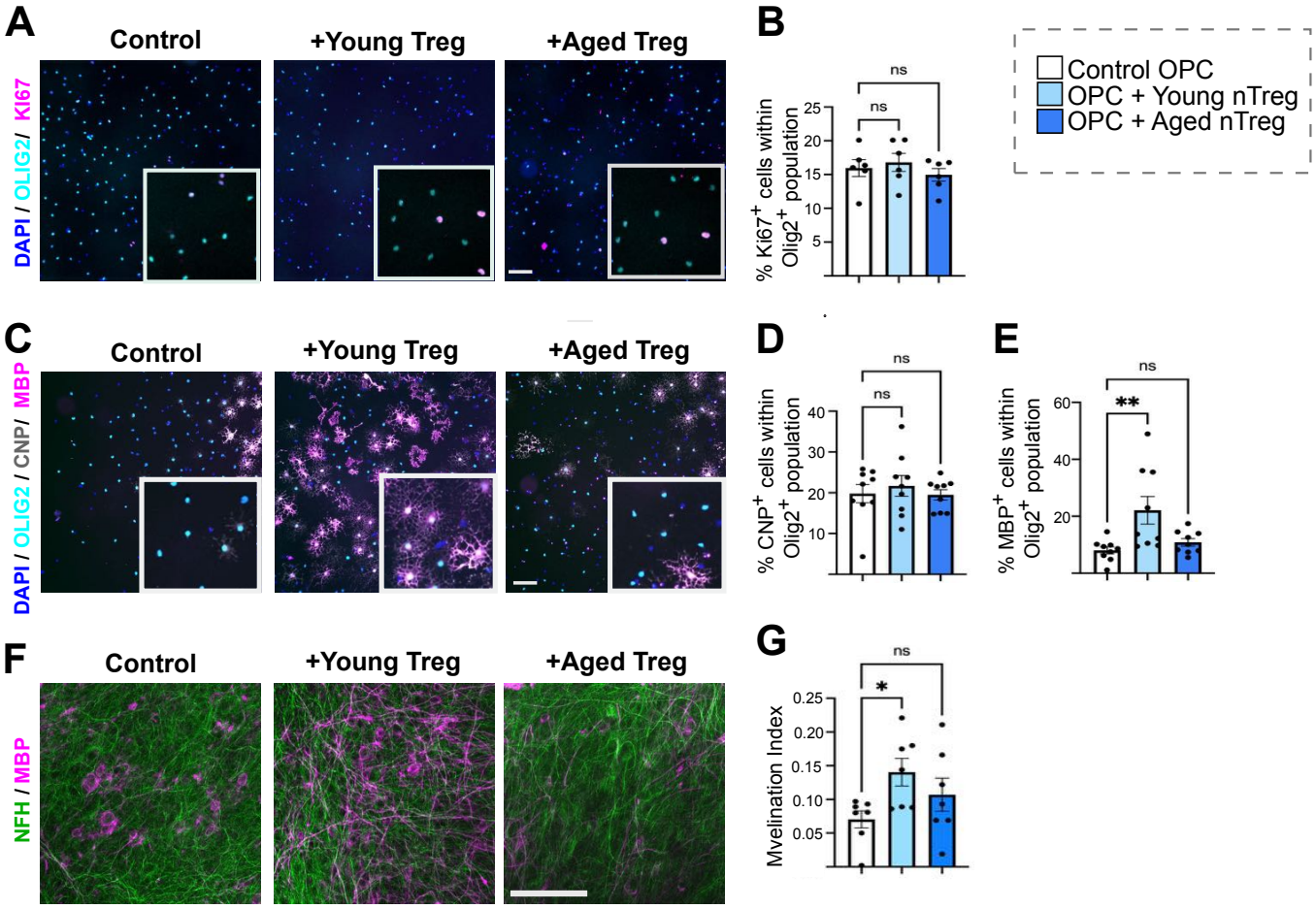


**Figure 2: Aged natural Treg demonstrate impaired capacity to drive OPC differentiation and myelination *in vitro.*** Representative images of OPCs co-cultured with young and aged nTreg and immunostained for OLIG2 (cyan) as a pan oligodendrocyte lineage marker, the proliferation marker Ki67 (magenta, **A**) and differentiation markers CNP (grey) and MBP (magenta) (**C**) (Scale bar = 100 µm). **B**) Quantification of OPC proliferation when co-cultured with young and aged nTreg (n=6, 1-way ANOVA after arcsin conversion) **D**) Quantification of the proportion of OPCs reaching early stage-differentiation when exposed to young and aged nTreg, as indicated by CNPase staining (n=9, 1-way ANOVA after arcsin conversion). **E**) Quantification of the proportion of OPCs expressing late-stage differentiation marker MBP in control and OPCs treated with young and aged nTreg (n=9, 1-way ANOVA, Sidak's multiple comparisons test). **F**) Immunohistochemistry of control and young and aged nTreg treated cerebellar slices (MBP, magenta and NFH, green, Scale bar = 100 µm). (**G**) Quantification of myelination index (ratio between MBP and NFH colocalization area and NFH area) in neonatal cerebellar slices (n=7, 1-way ANOVA after arcsin conversion, Sidak's multiple comparison tests). .

**Fig. 2**

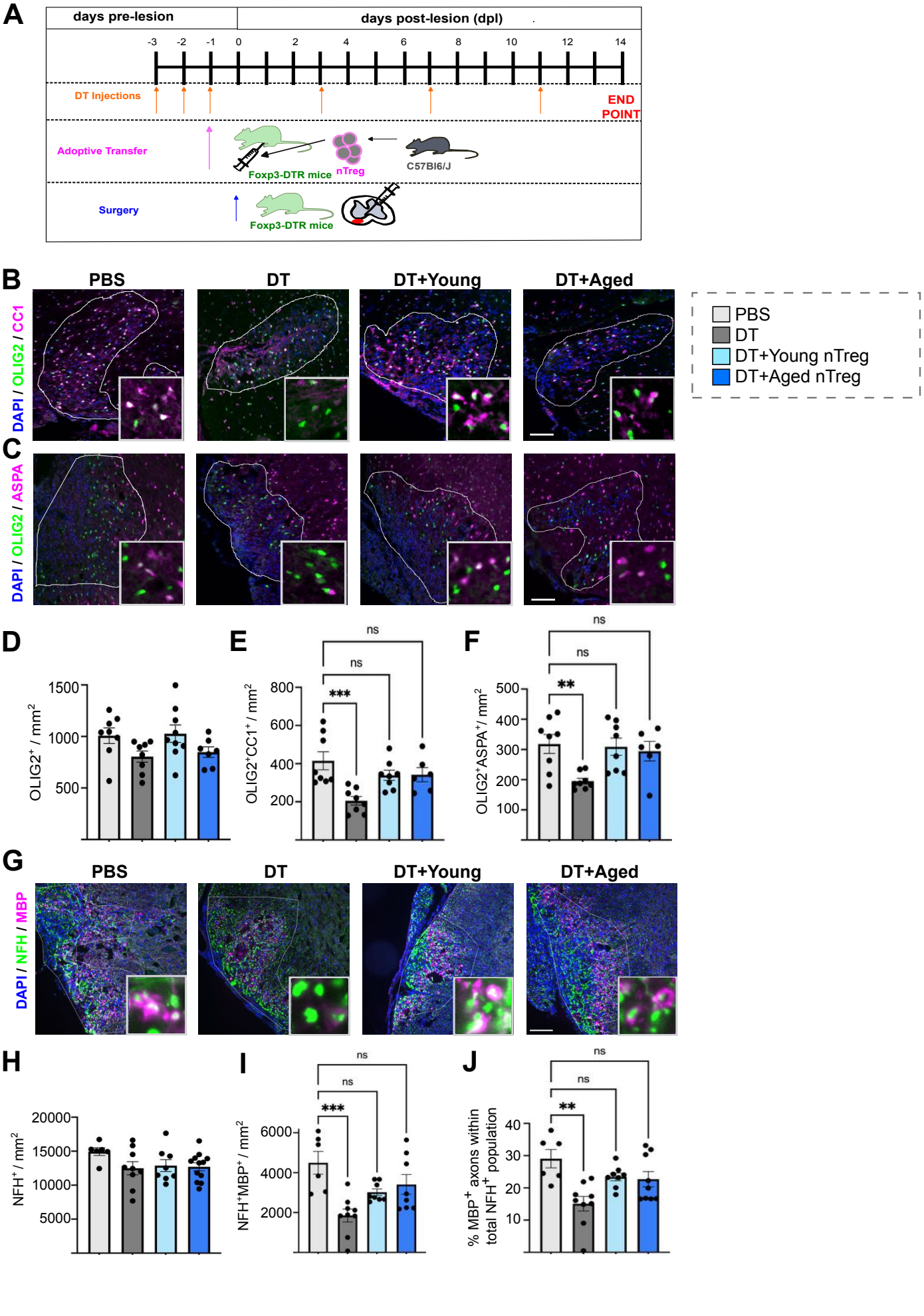


**Fig. 3**

**Figure 3: Myelin-regenerative capacity of aged Treg is restored in a young environment. A**) Diagram explaining the experimenta design of *in vivo* Treg depletion, Treg adoptive transfer and spinal cord demyelination. Representative iamges of immunostaining identifying oligodendrocytes by the co-localisation of the pan-oligodendrocyte lineage marker OLIG2 (green) with CC1 (magenta, **B**) or ASPA (magenta, **C**) at 14dpl (scale bar=100µm, demyelinated area is highlighted by the white line). Bar graphs show the quantification of total number of oligodendrocyte lineage cells (**D**), as well as CC1-expressing (**E**) or ASPA-expressing (**F**) oligodendrocytes in the demyelinated lesions of PBS control mice, natural Treg-depleted mice and mice depleted of endogenous Treg that received young or aged natural Treg by adoptive transfer (n=7-9, 1-way ANOVA, Sidak's multiple comparisons test). **G**) Representative images of immunostaining for neurofilament-H (NFH, green) and MBP (magenta) to quantifiy myelin wrapping as an early marker of remyelinationg at 14dpl (scale bar = 100µm, demyelination area is highlighted by the white line). Quantification shows the total number of axons (**H**), the density of MBP wrapped axons (**I**) and the percentage of MBP-wrapped axons from the total number of axons (**J**) (n=6-9, 1-way ANOVA, Sidak's multiple comparisons test).

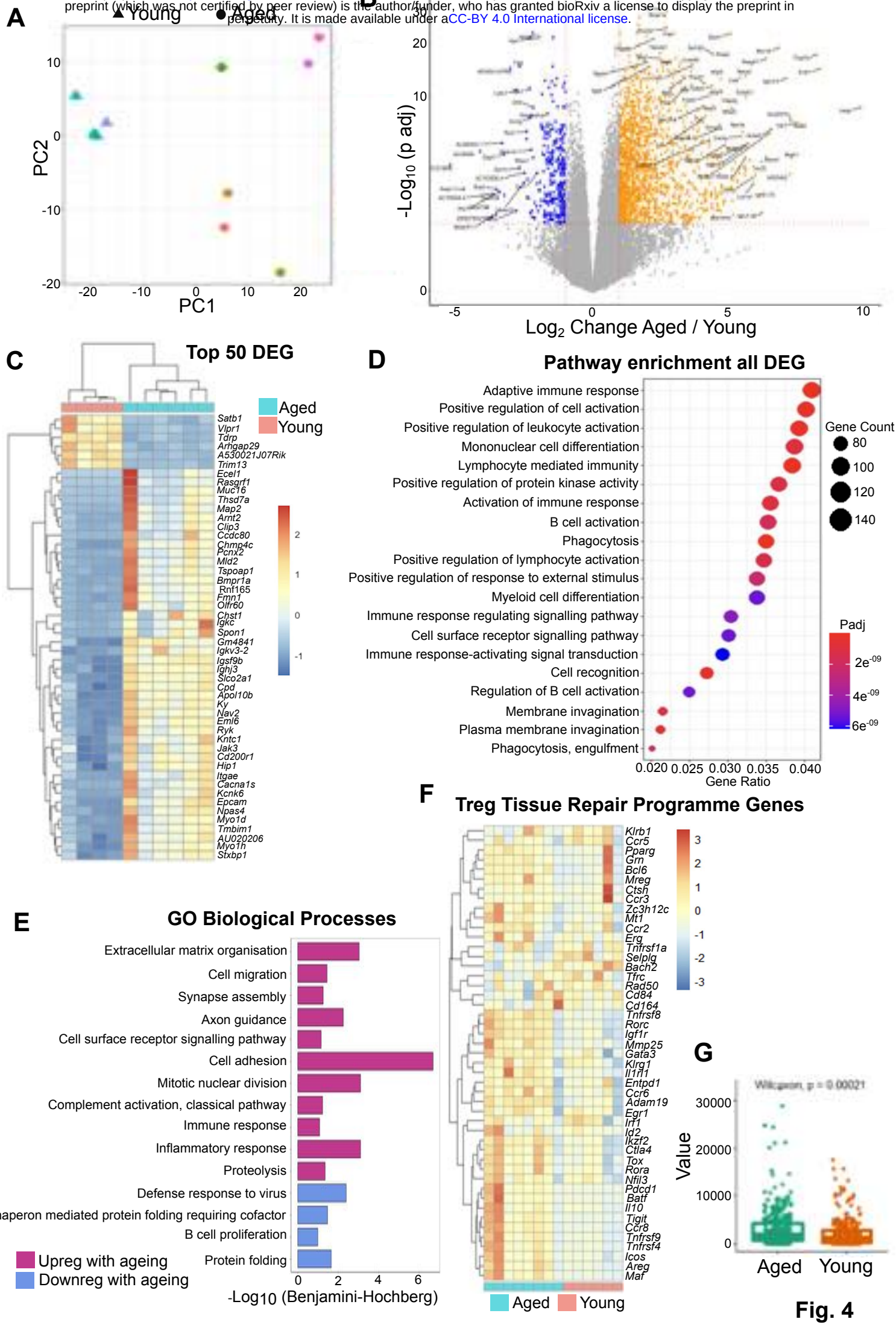


**Fig. 4**

**Figure 4: Ageing significantly alters natural Treg transcriptome. A**) Principal component analysis demostrating the clustering differences bedtween young and aged natural Treg. **B**) Volcano plot demostrating 1456 genes upregulated and 302 genes genes downregulated genes natural Treg relative to young Treg. **C**) Heatmap demonstrating hierarchical clustering of the top 50 differentially expressed genes between young and aged Treg. **D**) Graph showing the pathways enriched amongst differntially expressed genes. **E**) Bar graph highlighting the GO biological processes associated with genes that are upregulated or downregulated in aged Treg. **F**) Heatmap showing the normalised count values for the Treg tissue repair programme identified by Delacher *et al*.[23]. **G**) Graph showing the Treg tissue repair programme signature genes score in aged and young natural Treg.

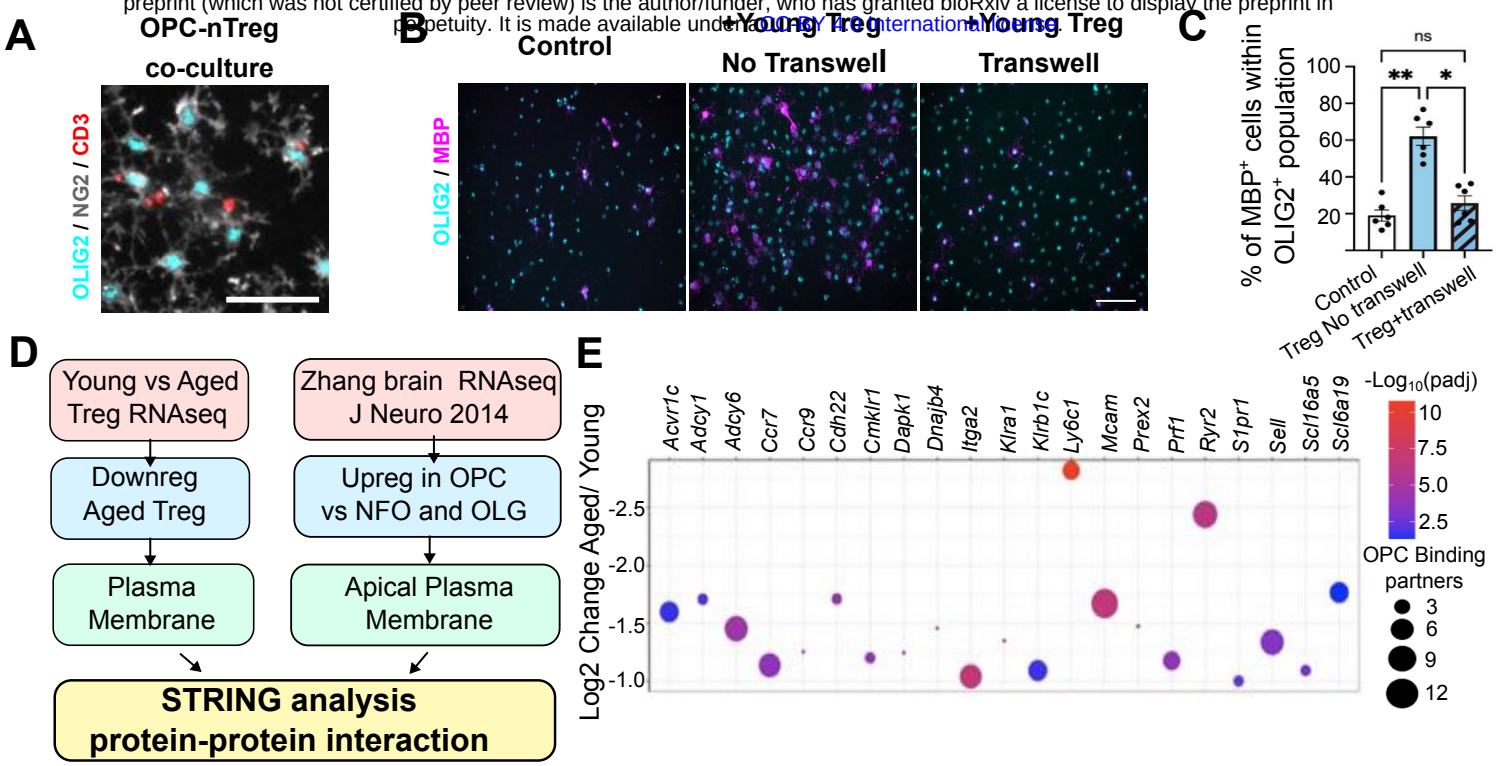


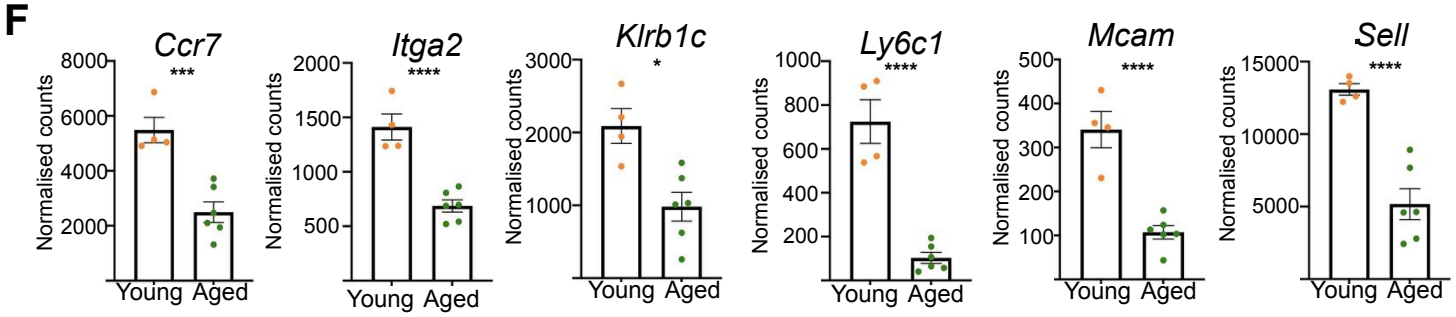


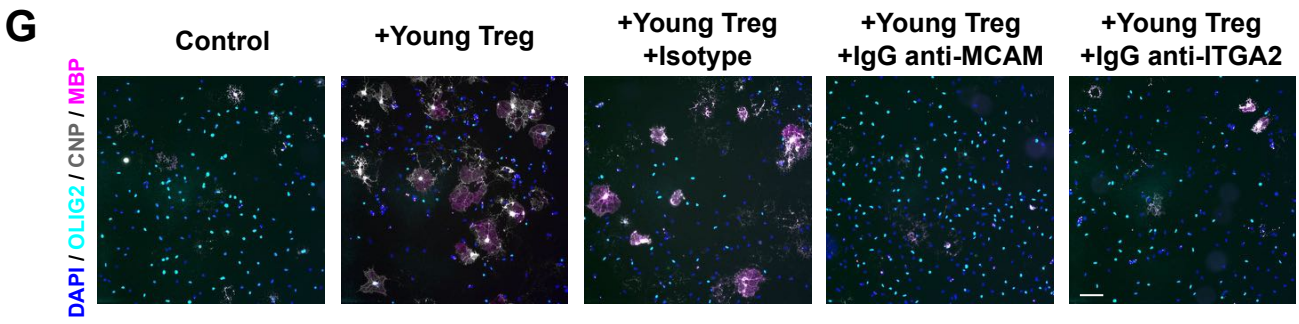


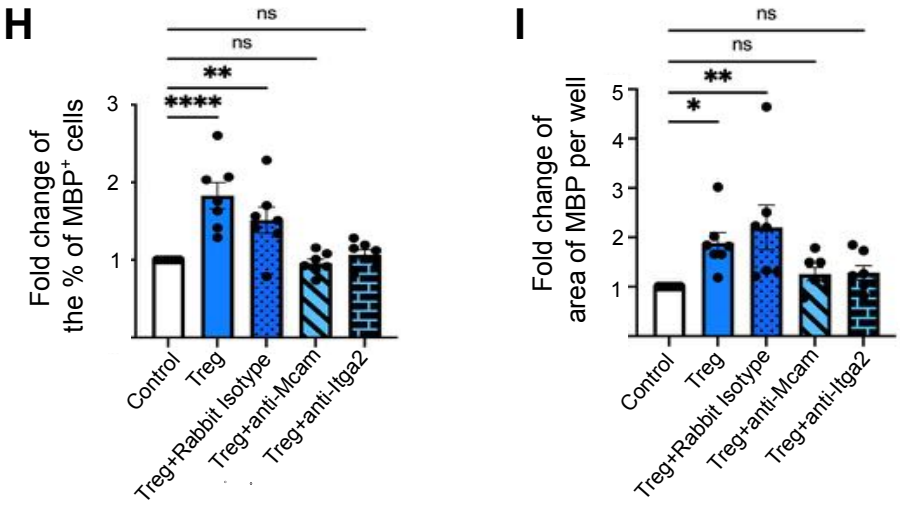


**Fig. 5**

**Figure 5: Mcam and Itga2 contribute to Treg-driven OPC differentiation and are downregulated in aged Treg.** **A**) Representative images of immunostaining showing cell-to-cell contact between OPCs and Treg in OPC-Treg co-cultures *in vitro*. OPCs are identified by the co-staining of OLIG2 (cyan) and NG2 (grey), while Treg are identified by CD3 (red) (scale bar = 50 µm). **B**) Representative images of immunostaining and **C**) quantification of MBP-expressing oligodendrocytes in control OPCs, OPCs directly co-cultured with young Treg and OPCs cultured with young Treg in a transwell (n=6, 1-way ANOVA after arcsin conversion, Sidak's multiple comparison's test). **D**) Diagram summarising bioinformatic approaches to identify protein-protein interactions between OPCs and Treg. **E**) Graph showing 21 protein candidates expressed in the nTreg plasma membrane, that are downregulated in aged nTreg and have potential bindings partners enriched in OPCs vs oligodendrocytes. $Log_2$ Change, $-Log_{10}$ (Padj) and the number of OPC binding partners are indicated (see legend). **F**) Bar graphs showing RNAseq normalised count values for the top 6 candidates. **G**) Representative images of immunostaining showing OPC differentiation in co-culture with young Treg in the presence ofr absence of neutralising antibodies against candidate cell surface mediators (scale bar=100µm). Bar graphs showing the quantification of OPC differentiation measured by the fold change in percentage of $MBP^+$ cells (**H**) and $MBP^+$ area per well (**I**) (n=7, 2-way ANOVA, Dunnett{s multiple comparsion tests).